International Journal of GEOMATE, June, 2025 Vol.28, Issue 130, pp.96-103
ISSN: 2186-2982 (P), 2186-2990 (O), Japan, DOI: https://doi.org/10.21660/2025.130.4923
Geotechnique, Construction Materials and Environment

NUMERICAL INVESTIGATION OF THE BEHAVIOR OF BOLTED STAINLESS-STEEL BEAM-TO-COLUMN JOINT

*Xuan Bang Nguyen[1], Cong Binh Dao[1] and Viet Chinh Mai[1]

[1]Institute of Construction Technology, Le Quy Don Technical University, Hanoi, Vietnam

*Corresponding Author, Received: 18 Feb. 2025, Revised: 02 April 2025, Accepted: 04 April 2025

ABSTRACT: This study presents a numerical investigation into the moment-rotation behavior of bolted stainless-steel beam-to-column joints using Finite Element (FE) modeling in ABAQUS, validated against experimental data. A series of numerical models is developed to assess the influence of angle cleat thickness (t_a), angle cleat leg length (L) parallel to the column flange, and column flange thickness (t_c) on joint performance. The results demonstrate that increasing ta from 10 mm to 16 mm enhances the maximum moment capacity (M_u) by 18.0%, indicating a significant improvement in load resistance. Conversely, extending L from 80 mm to 140 mm reduces M_u by 16.1%, while increasing rotational capacity by 80.4%, highlighting improved deformation capacity before failure. Changes in t_c exhibit a relatively minor effect, with a negligible influence on overall joint strength. These findings provide critical insights into the design and optimization of stainless steel connections, contributing to the development of more efficient and reliable structural applications.

Keywords: Stainless steel, Beam-to-column joint, Simulation method, Moment-rotation, Bolts

1. INTRODUCTION

Stainless steel is widely used in construction due to its excellent corrosion resistance, high durability, and aesthetic appeal. It is commonly applied in bridges, building facades, structural joints, marine or industrial environments, where long-term performance and low maintenance are critical [1-4]. Unlike carbon steel, stainless steel exhibits high strain hardening and nonlinear stress-strain behavior, which can enhance the rotational capacity of structural joints. However, current design codes, including Eurocode 3, primarily developed for carbon steel, often provide overly conservative estimates for stainless steel connections [5].

A few extensive studies have been conducted on stainless steel components, but investigations specifically targeting beam-to-column connections remain limited. Elflah's experimental study examined the structural behavior of stainless steel beam-column joints through six full-scale tests conducted on different joint typologies under static monotonic loading. The study's findings, along with a comprehensive evaluation of its contributions to the design of stainless steel structures, are presented [6]. Yuan et al. (2018) provided the first reported test data of stainless steel T-stubs. Test data includes bolt dimensions, material classification, T-stub depth, and preloading effects [7]. The joint of beam-to-concrete-filled hollow columns connected by bolts were later investigated by Tao et al. (2017), demonstrating the influence of concrete infill on joint response [8]. However, due to the interaction between concrete and blind bolts, their findings are not directly applicable to stainless steel joints without concrete infill. A numerical study on top and seat cleat connections was attempted by Hasan et al. (2017) [9]. Using Finite Element (FE) modelling in ABAQUS, the study developed and validated numerical models based on experimental data. The influence of strain hardening, a characteristic feature of austenitic stainless steel, was incorporated into the FE simulations. Talja et al. (2014) conducted a comprehensive experimental program on bolted connections made of ferritic stainless steel, with covering thicknesses between 0.5 mm and nearly 5 mm, encompassing multiple failure mechanisms [10]. Their findings confirmed the applicability of carbon steel design guidelines to stainless steel connections. Recent studies have advanced the understanding of cold-formed stainless steel bolted connections, particularly under elevated temperature conditions [11-14]. Numerical and experimental investigations have been conducted on both single shear and double shear bolted joints, highlighting the effects of temperature on strength degradation and failure modes. Finite element models, validated against test results, have demonstrated reliable predictions of connection behavior and enabled extensive parametric studies across varying temperature levels. These studies proposed modified bearing strength equations and reduction factors, improving the accuracy of existing American, Australian/New Zealand, and European design codes. Furthermore, comparative results showed that among the examined grades, austenitic stainless steel EN 1.4571 (AISI 316Ti) exhibited superior performance at elevated temperatures, while current design predictions remained generally conservative. Overall, the findings support the need for temperature-dependent design rules and emphasize the importance of incorporating material degradation

into strength evaluations of stainless steel connections. The study of Zuo et al. investigates double-lap shear behavior of WAAM 3D-printed austenitic stainless steel bolted connections [15]. Testing 43 specimens, it evaluates the impact of geometric and surface variables. Results show that AISC 360–22 predicts connection strength accurately when bolt hole deformation is considered.

2. RESEARCH SIGNIFICANCE

This study addresses the gap in understanding the structural performance of bolted stainless-steel beam-to-column joints, which behave differently from carbon steel due to nonlinear material properties. Using finite element modeling, the research evaluates full joint behavior, accounting for material nonlinearity, contact behavior, and bolt interaction. This study is unique in its use of advanced numerical modeling techniques to comprehensively evaluate the behavior of bolted stainless-steel beam-to-column joints, unlike previous research, which primarily examined individual components. The obtained results offer valuable insights for enhancing design guidelines and stainless steel structural reliability.

3. FINITE ELEMENT MODEL DEVELOPMENT

The FE model is developed using ABAQUS Explicit, a comprehensive software suite utilized for simulating the behavior of various materials and structures under different conditions [16-19]. Material properties for stainless steel are defined using the Ramberg–Osgood model to capture its nonlinear stress-strain behavior. The Ramberg-Osgood material model is a widely used nonlinear formulation for describing the stress-strain relationship of materials exhibiting strain hardening, particularly stainless steel and aluminum alloys [20]. The two-stage Ramberg-Osgood model, as adopted in Eurocode 3 [5], enhances accuracy by utilizing distinct expressions for the elastic and plastic regions, making it particularly suitable for predicting the mechanical behavior of stainless steel under large-strain conditions.

Table 1. Material properties in the simulation [6]

Component	Elastic modulus (GPa)	Yield strength /Ultimate strength (MPa)	n	m	ε_f
Flange	196.5	248/630	5.2	2.4	0.66
Web	205.7	263/650	6.7	2.4	0.65
Angle cleat	192.8	289/656	10.6	2.5	0.56
Bolt - M16	191.5	617/805	17.2	3.7	0.12

The material parameters of the stainless steel are shown in Table 1, where n and m represent the strain-hardening exponents utilized in the Ramberg-Osgood model. ε_f represents the uniaxial plastic strain at the point of fracture [21, 22].

All structural members are assigned by 8-node brick elements (C3D8R). Mesh sensitivity analyses determined optimal mesh sizes of 8 mm to 10 mm near the joint region, ensuring accurate stress distribution while maintaining computational efficiency. Fig. 1 illustrates the 3D model and element meshing of the stainless steel frame joint. In the simulation model, boundary conditions included fixed supports at the column base to replicate real constraints. Monotonic loading is applied incrementally at the beam tip to simulate progressively increasing bending moments. Contact interactions between bolts, steel plates, and column flanges are defined using frictional properties, capturing the load distribution and deformation mechanics within the connection. The coefficient of friction employed in numerical simulations typically ranges from 0.2 to 0.33, depending on surface roughness and material conditions [23-25]. In this study, a value of 0.29 is selected. Additionally, the bolt shank and clearance hole are connected using a finite slip approach, which enables the simulation of relative movement between components.

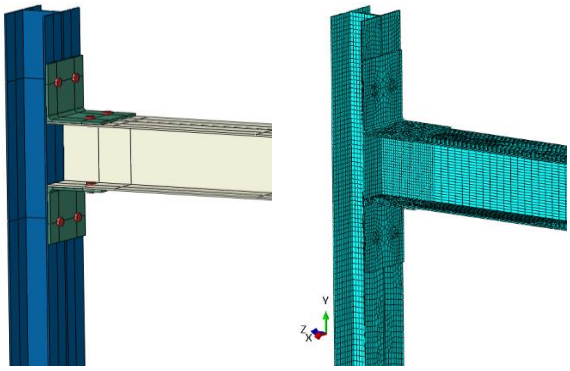

(a) (b)

Fig. 1 3D simulation (a) and mesh (b) model of stainless-steel beam-to-column joint

4. RESULTS AND DISCUSSIONS

4.1 Simulation model validation

The purpose of this section is to validate the accuracy of the developed numerical model by comparing its results with the experimental data. The study conducted by Elflah [6] was selected for the validation process. In Elflah's research, a stainless steel beam-to-column connection of the top and seat angle cleat connections (TSAC-O) type was subjected until failure. Fig. 2 presents the details of the connection. The connection consists of an I-

section column and beam, with the overall column depth of 240 mm, flange width of 120 mm, and flange thickness of 12 mm. The connection employs bolted angle cleats with thicknesses of 10 m. The bolts, with a diameter of 18 mm, are arranged in pairs and spaced 100 mm apart along the vertical axis. The horizontal bolt spacing on the column flange is 25 mm. The top and bottom angle cleats are bolted directly to the column flange, with their legs extending horizontally and vertically to secure the beam flanges. The horizontal leg of the angle cleats has a length of 60 mm, while the vertical leg is bolted with spacing of 35 mm between the bolts. Austenitic stainless steel and Grade A80 high-strength bolts were utilized in Elflah's test, as detailed in Table 2. Monotonic loading is applied at the end of the beam.

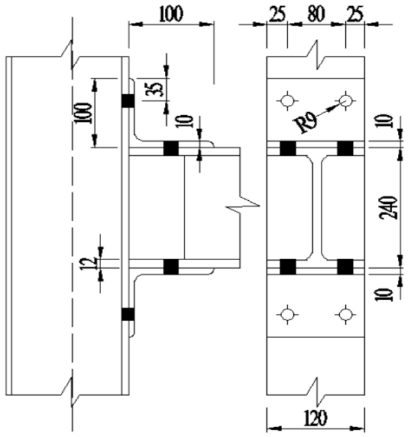

Fig. 2 Details of bolted stainless-steel beam-to-column joint [6]

Table 2. Material properties in the test of Elflah [6]

Sample	Elastic modulus (GPa)	Yield strength (MPa)	Ultimate strength (MPa)
Flange I-240×120×12	196.5	248	630
Web I-240×120×12	205.7	263	650
Bolt of M16 A80	192.8	617	805

The comparison between the experimental and simulation results is illustrated through the moment-rotation curve in Fig. 3 and the numerical summary in Table 3. The moment-rotation curves from both the experimental test and simulation demonstrate similar trends, characterized by an initial linear elastic phase, followed by plastic deformation, and culminating in failure. The experiment recorded a maximum moment of 41.5 kN·m, while the simulation predicted a higher value of 44.6 kN.m. The disparity between the two is 1.08, representing a difference of approximately 8%. This difference can be attributed to the idealization of material properties and boundary conditions in the numerical model, which may enhance the load-carrying capacity. The test showed a rotation of 162 mrad at M_u, whereas the simulation predicted 178.4 mrad, with a disparity factor of 1.1. This indicates that the simulation predicts slightly greater rotational ductility. The comparison confirms that the numerical model provides a good agreement of the structural performance compared to the TSAC-O-10 joint in the test of Elflah. The observed deviations are within acceptable limits, making the model a reliable tool for predicting the loading capacity of stainless joints in practical design applications.

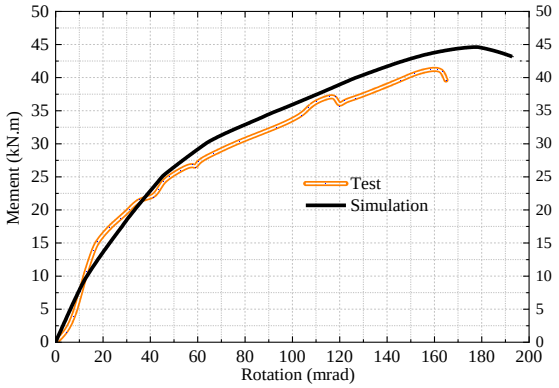

Fig. 3 Moment-rotation results according to the test of Elflah [6] and simulation

Table 3. Comparison between experimental and simulation results

Analytical method	Maximum moment M_u (kN.m)	Rotation φ at M_u (mrad)
Experiment (1)	41.5	162
Simulation (2)	44.6	178.4
Disparity (1)/(2)	1.08	1.1

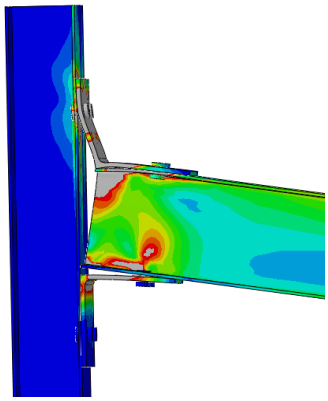

Fig. 4 Failure pattern of the stainless joint.

Fig. 4 presents the deformation pattern and failure mode of the numerical simulation. Compared to the test result for the bolted stainless steel beam-to-column joint, the numerical simulation shows significant bending and yielding in the top angle cleat, particularly near the bolt connections and the interface with the column flange. The beam exhibits considerable rotation, causing the cleat to undergo plastic hinge formation before failure. Serious damage is primarily localized around the upper bolt row and the cleat-column connection region, suggesting that these are the critical locations for structural failure. The final stage of deformation results in large out-of-plane displacement of the beam and severe inelastic deformation of the angle cleat, leading to overall joint failure. Simulation model result is consistent with the observed failure mode in the experiment of Elflah [6].

4.2 Stress results

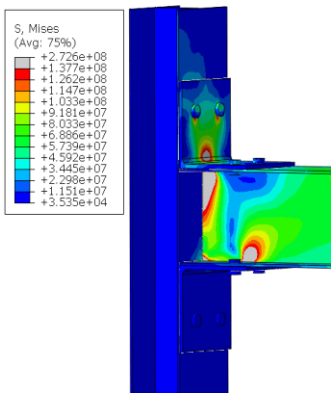

(a) Initial loading stage

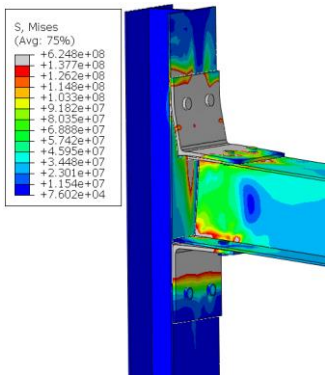

(b) Ultimate loading stage

Fig. 5 Stress distribution in the bolted stainless-steel beam-to-column joint

Fig. 5 shows the von Mises stress distribution within the bolted stainless-steel beam-to-column joint under progressively increasing load, revealing critical stress concentration zones and deformation patterns. At the initial loading phase, the stress distribution remains relatively uniform, with moderate concentrations near the bolt connections and the interface between the beam flange and column flange, indicating that the connection is still within its elastic range. The stress at this stage is approximately 2.72×10^8 Pa, primarily concentrated around the bolt holes and the angle cleat, with no significant deformations observed. As the applied load increases, stress magnitudes rise, with localized stress intensification observed at the upper bolt row and top angle cleat, marking the onset of plastic deformation. At this intermediate stage, the connection experiences a transition from elastic to plastic behavior, with yielding beginning in high-stress regions, particularly along the column flange and the beam flange near the connection interface. The moment-rotation relationship indicates a reduction in joint stiffness as plastic deformation progresses, suggesting a shift in load distribution within the connection. In the ultimate loading phase, extensive plastic deformation occurs, particularly in the top angle cleat, bolt holes, and beam flange, leading to peak stress values of 6.24×10^8 Pa and significant structural distortions. The final stage is characterized by plastic hinge formation near the joint, with substantial yielding along the column flange and localized bolt bearing failure, ultimately resulting in joint failure. The observed stress distribution highlights the ductile behavior of stainless steel, allowing for gradual yielding rather than sudden brittle failure, which is crucial for seismic-resistant and energy-dissipating structures.

The von Mises stress distribution in bolts of the stainless-steel beam-to-column joint under different loading stages is depicted in Fig. 6. The numerical simulation results indicate a gradual increase in stress levels, with critical stress accumulation zones shifting as loading progresses. At the initial loading stage (Fig. 6a), stress concentrations are primarily localized around the contact regions between the bolt shank and the bolt hole, as well as the connected plate. The peak von Mises stress at this stage is approximately 2.47×10^8 Pa, indicating that the bolt is still within its elastic deformation range. As loading increases to the intermediate stage (Fig. 6b), stress levels intensify, particularly along the shank of the bolt and at the contact surface with the connected plates. The bearing stress at the bolt-hole interface increases, leading to local plastic deformations in the surrounding material. The maximum stress at this stage reaches approximately 6.0×10^8 Pa. The bolt is experiencing localized yielding, particularly near the bolt-head. At the ultimate loading stage (Fig. 6c), severe plastic deformations occur. The stress reaches a peak value

of approximately 7.90 × 10^8 Pa, nearly reaching the ultimate tensile strength of bolt's material, leading to significant deformation and potential failure.

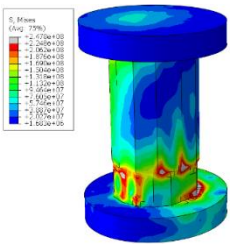

(a) Initial loading stage

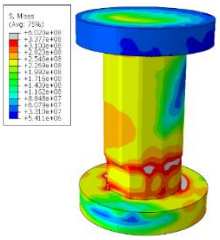

(b) Intermediate loading stage

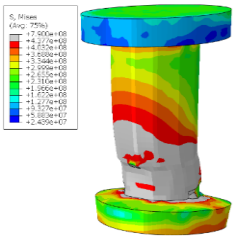

(c) Ultimate loading stage

Fig. 6 Stress distribution in the bolts

4.3 Parametric study

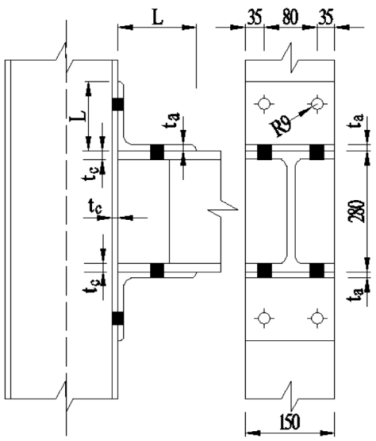

Fig. 7 Details of parametric studies in the simulation

In this section, the parametric study is conducted based on the validated numerical model. The selected parameters for analysis include the angle cleat thickness (t_a), the column flange/face thickness (t_c), and the length of the angle cleat leg parallel to the column flange (L), as illustrated in Fig. 7. The determination of the structural member thickness and the detailed joint configuration is based on the guidelines and recommendations outlined in EN 1993-1-8 [5].

Table 4 presents the parametric variations of the angle cleat thickness (t_a) while maintaining other geometric parameters constant. The study considers four cases, systematically reducing t_a from 16 mm to 10 mm to assess its influence on the moment-rotation behavior of bolted stainless steel beam-to-column joints. The column flange thickness (t_c) is fixed at 12 mm, and the length of the angle cleat leg parallel to the column flange (L) is maintained at 120 mm across all cases. Additionally, the flange dimensions of structural members remain consistent at 280 × 150 × 12 mm for both the beam and the column to ensure that the variations in response are solely attributed to the changes in t_a. This parametric approach allows for a comprehensive evaluation of how angle cleat thickness affects the joint's stiffness, moment capacity, and rotation capacity while minimizing the influence of other geometric factors.

Table 4. Variation of angle cleat thickness (t_a) in parametric studies

Case study	t_a (mm)	t_c (mm)	L (mm)	Flange of structural members (mm)
Case 1	16	12	120	280×150×12
Case 2	14	12	120	280×150×12
Case 3	12	12	120	280×150×12
Case 4	10	12	120	280×150×12

The parametric analysis reveals a significant influence of angle cleat thickness (t_a) on the moment-rotation behavior of bolted stainless steel beam-to-column joints, as shown in Table 5 and Fig. 8. As the angle cleat thickness ta increases, the maximum moment capacity (M_u) also increases, reaching 56.14 kN·m at t_a = 16 mm (baseline case) and decreasing by 6.8%, 11.9%, and 18.0% for ta = 14 mm, 12 mm, and 10 mm, respectively. This trend indicates that thicker angle cleats enhance load-bearing capacity, as they provide greater stiffness and resistance to deformation. However, this increase in strength results in the higher of rotation capacity (φ at M_u). Specifically, φ increases by 23.1%, 49.6%, and 81.5% for t_a = 14 mm, 12 mm, and 10 mm, respectively, compared to the baseline case (t_a = 16 mm). The moment-rotation curves further illustrate that thicker angle cleats lead to steeper initial slopes, indicating higher stiffness, while thinner cleats allow for greater deformation before failure, contributing to enhanced ductility. This relation between strength and flexibility aligns with existing experiment results on stainless steel

connections [6], confirming that thicker cleats lead to earlier bolt failure due to higher force transfer, whereas thinner cleats experience significant inelastic bending before ultimate failure. From a design perspective, thicker angle cleats (t_a = 16 mm, 14 mm) are preferable for rigid connections, whereas thinner cleats (t_a = 12 mm, 10 mm) are more suitable for applications requiring energy dissipation and rotational flexibility, such as seismic-resistant structures.

Table 5. Moment and rotation results for different values of angle cleat thickness

Case study	t_a (mm)	M_u (kN.m)	Reduction of M_u (%)	Rotation φ (mrad) at M_u	Increment of φ (%)
Case 1	16	56.14	//	133.62	//
Case 2	14	52.33	6.8	164.44	23.1
Case 3	12	49.47	11.9	199.88	49.6
Case 4	10	46.05	18.0	242.52	81.5

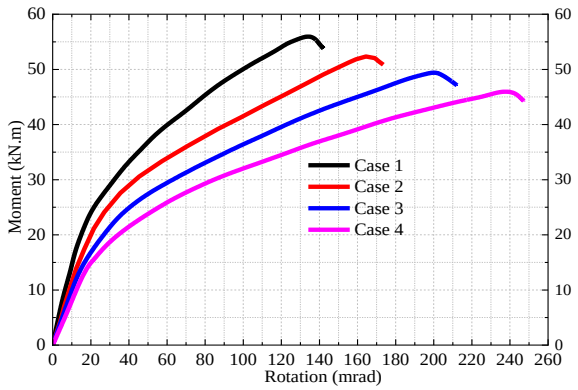

Fig. 8 Moment-rotation curve for varying angle cleat thickness

Table 6. Variation of angle cleat leg length (L) parallel to the column flange

Case study	t_a (mm)	t_c (mm)	L (mm)	Flange of structural members (mm)
Case 5	12	12	80	280×150×12
Case 6	12	12	100	280×150×12
Case 7	12	12	120	280×150×12
Case 8	12	12	140	280×150×12

Table 6 presents the parametric variation of length (L), which is adjusted across four cases to evaluate its influence on the moment-rotation behavior of bolted stainless steel beam-to-column joints. In all cases, the angle cleat thickness (t_a) and column flange thickness (t_c) remain constant at 12 mm, ensuring that the observed effects are solely attributed to changes in L. The study considers L values ranging from 80 mm to 140 mm. The flange dimensions of the structural members are maintained at 280 × 150 × 12 mm for both the beam and the column, ensuring consistency in geometric parameters.

Results of parametric study that investigates the influence of angle cleat leg length (L) parallel to the column flange on the moment-rotation behavior of bolted stainless steel beam-to-column joints is shown in Table 7 and Fig. 9. It is observed that as L increases, the maximum moment capacity (M_u) decreases, while the rotation at maximum moment (φ at M_u) increases. Specifically, M_u decreases from 54.31 kN·m at L = 80 mm to 45.56 kN·m at L = 140 mm, corresponding to a 16.1% reduction. The experimental investigations conducted by Elflah et al. (2018) and Hasan et al. (2017) on the influence of L on moment-rotation capacity exhibited a similar trend to that observed in the present study. This decline is attributed to the longer cleat leg reducing the lever arm efficiency, leading to lower stiffness and moment resistance. Conversely, the rotation capacity exhibits a substantial increase, with φ at Mu rising from 142.2 mrad to 256.5 mrad, representing an 80.4% increase. The moment-rotation curves further illustrate that shorter cleats (L = 80 mm, 100 mm) result in steeper initial slopes, indicating higher stiffness, whereas longer cleats (L = 120 mm, 140 mm) allow for greater deformation before failure.

Table 7. Moment and rotation results for different values of L

Case study	L (mm)	M_u (kN.m)	Reduction of M_u (%)	Rotation φ (mrad) at Mu	Increment of φ (%)
Case 5	80	54.31	//	142.27	//
Case 6	100	49.47	8.9	199.88	40.5
Case 7	120	47.18	13.1	233.14	64.0
Case 8	140	45.56	16.1	256.55	80.4

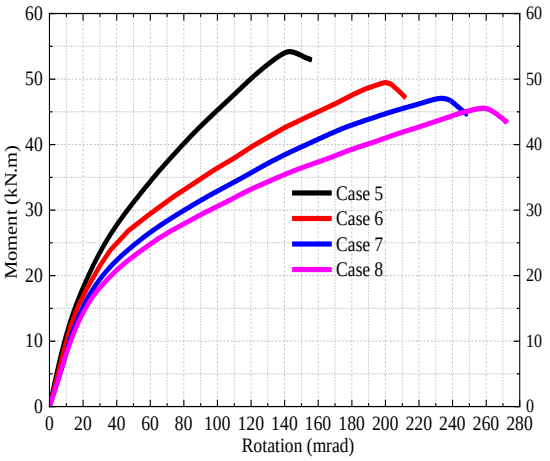

Fig. 9 Moment-rotation curve for varying L

Table 8. Variation of column flange thickness (t_c) in parametric studies

Case study	t_a (mm)	t_c (mm)	L (mm)	Flange of structural members (mm)
Case 9	12	16	120	280×150×16
Case 10	12	14	120	280×150×14
Case 11	12	12	120	280×150×12
Case 12	12	10	120	280×150×10

Table 8 shows the variation of column flange thickness (t_c) in the parametric study, examining its influence on the moment-rotation response of bolted stainless steel beam-to-column joints. The study considers four cases, decreasing t_c from 16 mm to 10 mm, while keeping other parameters constant (angle cleat thickness t_a = 12 mm, angle cleat leg length L = 120 mm, and flange dimensions of 280 × 150 × 12 mm). The purpose of this analysis is to evaluate how column flange stiffness affects joint strength, rotational capacity, and deformation behavior.

Table 9. Moment and rotation results for varying column flange thickness (t_c)

Case study	t_c (mm)	M_u (kN.m)	Reduction of M_u (%)	Rotation φ (mrad) at M_u	Increment of φ (%)
Case 9	16	51.22	//	175.05	//
Case 10	14	50.55	1.31	188.02	7.41
Case 11	12	49.47	3.42	199.88	14.18
Case 12	10	48.54	5.23	212.35	21.31

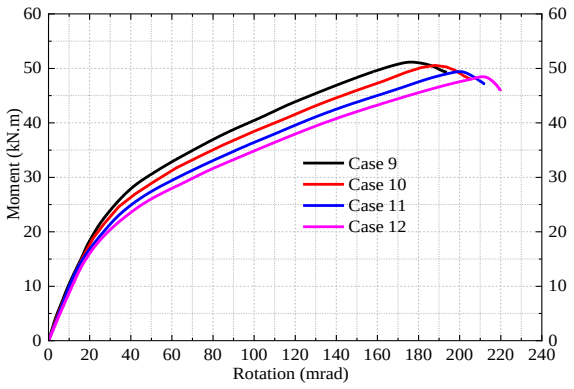

Fig. 10 Moment-rotation curve for varying column flange thickness (t_c)

The parametric study investigates the effect of column flange thickness (t_c) on the behavior of bolted stainless steel beam-to-column joints and highlights that its impact is notably lower compared to variations in thickness (t_a) length (L). As shown in Table 9 and Fig. 10, reducing t_c from 16 mm to 10 mm leads to a 5.23% decrease in maximum moment capacity (M_u) and a 21.31% increase in rotation at maximum moment (φ at M_u). This is relatively minor when compared to the influence of ta, where decreasing the cleat thickness resulted in a 14.86% reduction in M_u and an 81.5% increase in φ, or L, where increasing the cleat leg length led to a 16.1% drop in M_u and an 80.4% rise in φ. The moment-rotation curves further illustrate that modifying t_c does not fundamentally alter joint stiffness or deformation behavior, unlike ta and L, which have a more direct influence on the force transfer mechanism and plastic deformation patterns. While thinner column flanges allow for some increased flexibility, the overall effect on structural performance remains limited, suggesting that design optimization should prioritize modifications in t_a and L for achieving significant improvements in either moment resistance or ductility.

5. CONCLUSION

This study presents a comprehensive numerical investigation of bolted stainless steel beam-to-column joints, focusing on moment-rotation behavior and the influence of key geometric parameters. The following key conclusions can be drawn:

- The thickness of the angle cleat (t_a) and the length of the cleat leg (L) have a significant influence on the loading capacity of the joint. Increasing ta from 10 mm to 16 mm resulted in an 18.0% increase in maximum moment capacity (M_u). Conversely, extending L from 80 mm to 140 mm led to a 16.1% reduction in M_u, while increasing the rotation capacity by 80.4%, indicating that longer cleat legs enhance deformation capacity before failure but reduce overall joint rigidity.
- The column flange thickness (t_c) exhibited a relatively minor influence on joint performance. Reducing t_c from 16 mm to 10 mm resulted in only a 5.23% decrease in maximum moment capacity (M_u), while the rotation at M_u increased by 21.31%, indicating a limited effect on overall structural behavior. This finding indicates that optimizing t_c is less critical compared to modifications in ta and L for enhancing joint performance.

Future studies will focus on the parametric investigations of bolt configurations, strain-rate-dependent material modeling, and experimental validation under seismic loading or environmental exposure. These advancements will promote the use of stainless steel as a sustainable and high-performance material in modern structural applications.

6. REFERENCES

[1] Hlal F., Amani M., and Al-Emrani M., Stainless Steel Corrugated Web Girders for Composite Road Bridges: Optimization and Parametric Studies, Engineering Structures, Vol. 302, 2024, pp. 117366.

[2] Ghalla M., Alhaddad M., and Al-Azzawi W., Enhancing Shear Strength of RC Beams Through Externally Bonded Reinforcement With Stainless-Steel Strips and FRCM Jacket to Mitigate the Failure Risk, Results in Engineering, Vol. 22, 2024, pp. 102246.

[3] Duan S., Zhang S., and Yuan H., Numerical Study and Design of S35657 Stainless Steel Welded Stub Columns, Journal of Constructional Steel Research, Vol. 214, 2024, pp. 108473.

[4] De Carvalho A. S., and Silvestre N., Nonlinear Inelastic Stability Behavior of High-Strength Stainless Steel I-Beams With Sinusoidal Web Openings, International Journal of Structural Stability and Dynamics, Vol. 24, 2024, pp. 2450080.

[5] Standard B., Eurocode 3-Design of Steel Structures, 1993, pp. 2005.

[6] Elflah M. A. H., Structural Behaviour of Stainless Steel Bolted Beam to Column Joints, PhD Thesis, University of Birmingham, 2018.

[7] Yuan H., Rasmussen K. J. R., and Wang C., Experimental Behaviour of Stainless Steel Bolted T-Stub Connections Under Monotonic Loading, Journal of Constructional Steel Research, Vol. 152, 2019, pp. 213-224.

[8] Tao Z., Wang Z. B., Yu Q., and Uy B., Experimental Study on Blind Bolted Connections to Concrete-Filled Stainless Steel Columns, Journal of Constructional Steel Research, Vol. 128, 2017, pp. 825-838.

[9] Hasan M. J., Ashraf M., and Uy B., Moment-Rotation Behaviour of Top-Seat Angle Bolted Connections Produced From Austenitic Stainless Steel, Journal of Constructional Steel Research, Vol. 136, 2017, pp. 149-161.

[10] Talja A. and Torkar M., Lap Shear Tests of Bolted and Screwed Ferritic Stainless Steel Connections, Thin-Walled Structures, Vol. 83, 2014, pp. 157-168.

[11] Cai Y. and Young B., Bearing Factors of Cold-Formed Stainless Steel Double Shear Bolted Connections at Elevated Temperatures, Thin-Walled Structures, Vol. 98, 2016, pp. 212-229.

[12] Cai Y. and Young B., High Temperature Tests of Cold-Formed Stainless Steel Double Shear Bolted Connections, Journal of Constructional Steel Research, Vol. 104, 2015, pp. 49-63.

[13] Cai Y. and Young B., Structural Behavior of Cold-Formed Stainless Steel Bolted Connections, Thin-Walled Structures, Vol. 83, 2014, pp. 147-156.

[14] Cai Y. and Young B., Behavior of Cold-Formed Stainless Steel Single Shear Bolted Connections at Elevated Temperatures, Thin-Walled Structures, Vol. 75, 2014, pp. 63-75.

[15] Zuo W., Wang Z., and Chen S., Experimental Investigation on Double-Lap Shear Behavior of 3D Printed Austenitic Stainless Steel Bolted Connections, Engineering Structures, Vol. 317, 2024, pp. 118501.

[16] Dassault Systèmes, Abaqus/CAE User's Guide, 2016.

[17] Olarewaju A. J., Estimation of Blast Loads for Studying the Dynamic Effects of Coeffcient of Friction on Buried Pipes by Simulation, International Journal of GEOMATE, Vol. 7, Issue 13, 2014, pp. 1017-1024.

[18] Khassaf S. I., Chkheiwr A., and Jasim M. A., Effect of Contraction Joints on the Structural Performance of Arch Dam, International Journal of GEOMATE, Vol. 19, 2020, pp. 219-227.

[19] Akhmad R. H. P., Influence of Seawater on Strength of Concrete Beams Strengthened With Glass Fiber Reinforced Polymer Sheet, International Journal of GEOMATE, Vol. 26, Issue 117, 2024, pp. 35-42.

[20] Ramberg W. and Osgood W. R., Description of Stress-Strain Curves by Three Parameters, National Advisory Committee For Aeronautics, Washington DC, 1943.

[21] Eladly M. M., Behaviour of Stainless Steel Beam-to-Column Bolted Connections–Part 1: Simplified FE Model, Journal of Constructional Steel Research, Vol. 164, 2020, pp. 105784.

[22] Elflah M., Rasmussen K. J. R., and Young B., Behaviour of Stainless Steel Beam-to-Column Joints—Part 1: Experimental Investigation, Journal of Constructional Steel Research, Vol. 152, 2018, pp. 183-193.

[23] Wang Z.-Y. and Wang Q.-Y., Yield and Ultimate Strengths Determination of a Blind Bolted Endplate Connection to Square Hollow Section Column, Engineering Structures, Vol. 111, 2016, pp. 345-369.

[24] Massimo L., Kuhlmann U., and Lindner J., Experimental Analysis and Mechanical Modeling of T-Stubs With Four Bolts per Row, Journal of Constructional Steel Research, Vol. 101, 2014, pp. 158-174.

[25] Liu Y., Málaga-Chuquitaype C., and Elghazouli A., Behaviour of Beam-to-Tubular Column Angle Connections Under Shear Loads, Engineering Structures, Vol. 42, 2012, pp. 434-456.